Elucidating the Breathing of the Metal–Organic Framework MIL-53(Sc) with ab Initio Molecular Dynamics Simulations and in Situ X-ray Powder Diffraction Experiments

Cite as:
Chen, L., Mowat, J. P. S., Fairen-Jimenez, D., Thompson, S. P., Morrison, C., Wright, P. A., & Düren, T. (2013). Elucidating the Breathing of the Metal–Organic Framework MIL-53(Sc) with ab Initio Molecular Dynamics Simulations and in Situ X-ray Powder Diffraction Experiments. *Journal of the American Chemical Society*, 135(42), 15763–15773.

Manuscript received: 07/04/2013; Accepted: 03/06/2013; Article published: 18/06/2013

Elucidating the Breathing of the Metal-Organic Framework MIL-53(Sc) with *ab initio* Molecular Dynamics Simulations and *in Situ* X-Ray Powder Diffraction Experiments**

Linjiang Chen,[1] John P. S. Mowat,[2] David Fairen-Jimenez,[3] Carole A. Morrison,[4] Stephen P. Thompson,[5] Paul A. Wright[2] and Tina Düren[1,*]

[1]Institute for Materials and Processes, School of Engineering, The University of Edinburgh, King's Buildings, Edin-burgh, EH9 3JL, UK.

[2]EaStCHEM School of Chemistry, University of St. Andrews, Purdie Building, North Haugh, St. Andrews, Fife, KY16 9ST, UK.

[3]Department of Chemical Engineering and Biotechnology, University of Cambridge, Pembroke Street, Cambridge, CB2 3RA, UK.

[4]School of Chemistry and EaStCHEM Research School, The University of Edinburgh, King's Buildings, Edinburgh, EH9 3JJ, UK.

[5]Diamond Light Source Ltd, Harwell Science and Innovation Campus, Didcot, Oxfordshire, OX11 0DE, UK.

[*]Corresponding author; e-mail: tina.duren@ed.ac.uk

[**]We thank the EPSRC for funding (EP/G062129/1) and Doctoral Prize funding (J.P.S.M.). D.F.-J. thanks the Royal Society funding through a University Research Fellowship. This work made use of the Edinburgh Compute and Data Facility (ECDF) (http://www.ecdf.ed.ac.uk) and the resources provided by HECToR (http://www.hector.ac.uk), made available through the ECDF. We acknowledge Professor Chiu C. Tang for assistance at the I-11 beamline at the Diamond Light Source (DLS) and DLS for beamtime.

Supporting information:
Computational details about the DFT calculations, DFT-based geometry optimization calcula-tions, and AIMD simulations. GCMC simulation details, generic force-field parameters for MIL-53(Sc) and CO2 atoms, and partial atomic charges for the MIL-53(Sc) framework. AIMD simulation-based modeling procedures for generating the various structural forms of MIL-53(Sc). Details about calculation of framework potential energy and pore-opening energy. Time evolution of the MIL-53(Sc)-int structure during the course of the AIMD simulation. Description of the MIL-53(Sc)-np structure and comparison with the int form. Details about the determination of the MIL-53(Sc)-lp structure via the energy minimization-based modeling approach in conjunction with the experimental unit cell parameters. This material is available free of charge via the Internet at http://pubs.acs.org

Graphical abstract:

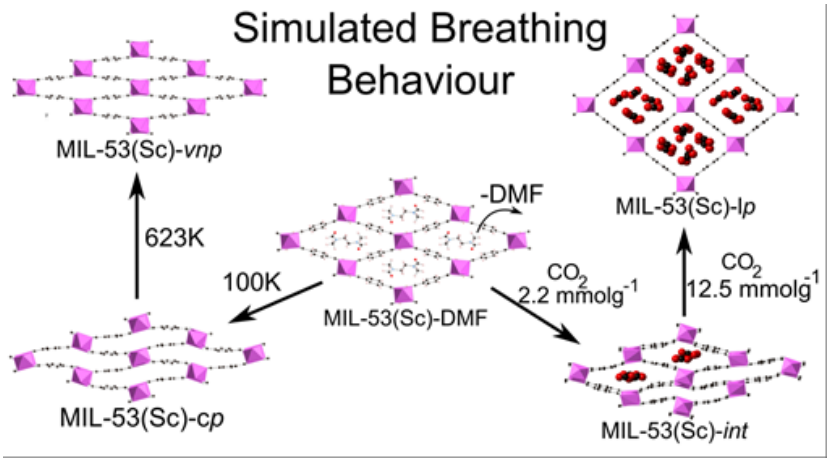

Keywords:

metal-organic framework, flexibility, breathing, ab initio molecular dynamics, and in situ X-ray powder diffraction

Abstract

Ab initio molecular dynamics (AIMD) simulation has been used to predict structural transitions of the breathing metal-organic framework (MOF) MIL-53(Sc) in response to changes in temperature over the range 100 – 623 K and adsorption of CO_2 from 0 – 0.9 bar at 196 K. The method has for the first time been shown to predict successfully both temperature-dependent structural changes as well as the structural response to variable sorbate uptake of a flexible MOF. AIMD employing dispersion-corrected density functional theory accurately simulates the experimentally observed closure of MIL-53(Sc) upon solvent removal and the transition of the empty MOF from the *closed-pore* phase to the *very-narrow-pore* phase (symmetry changes from $P\,2_1/c$ to $C\,2/c$) upon temperature increase, indicating that it is able directly to take account of entropic as well as enthalpic effects. Similar AIMD simulations were also deployed to mimic the CO_2 adsorption of MIL-53(Sc) *in silico* by allowing the MIL-53(Sc) framework to evolve freely in response to CO_2 loadings selected by reference to the experimental two-step adsorption isotherm. These AIMD simulations successfully predict and so enable the structure determination of the two CO_2-containing *intermediate* and *large-pore* phases observed by experimental synchrotron X-ray diffraction studies upon increasing CO_2 pressure: this would not have been possible for the *intermediate* structure via conventional methods because of diffraction peak broadening. Furthermore, the strong and anisotropic peak broadening observed for the *intermediate* structure is explained in terms of fluctuations of the framework predicted by the AIMD simulations. Fundamental insights from the molecular-level interactions further revealed the origin of the breathing of MIL-53(Sc) upon temperature variation and CO_2 adsorption. These simulations illustrate the power of the AIMD method for the prediction and understanding of the behavior of flexible microporous solids.

1. Introduction

Metal-organic frameworks (MOFs)[1] (also known as porous coordination polymers[2]) are hybrid porous solids that represent an extensive family of crystalline materials realized through a modular synthesis from metal centers and organic ligands. Breathing MOFs combine 'regularity' with 'softness' by exhibiting large, reversible structural deformation (softness) upon the action of various external physical (e.g., temperature or mechanical pressure) or chemical (e.g., guest-molecule inclusion) stimuli without losing crystallinity or bond breaking (regularity).[3,4] This phenomenon is characterized by pronounced reversible structural transitions between two (or more) states resulting from the expansion or contraction of the three-dimensional porous framework. The associated large variations in unit cell volume, sometimes as much as 40 to 270%,[5,6] give rise to promising applications of these breathing MOFs in numerous fields ranging from gas storage and separation to drug encapsulation and delivery.[7,8]

Among these soft porous solids, the trivalent metal (M^{3+}; M = Cr, Al, Fe, Sc, etc.) terephthalate MIL-53 (MIL stands for Materials of Institute Lavoisier) is one of the most widely studied of all MOFs, because of its ability to change crystal structure markedly in response to changing temperature and guest-molecule adsorption (Figure 1).[5,9-11] The compounds belonging to the MIL-53 family are built up from chains of μ_2-OH corner-sharing $MO_4(OH)_2$ octahedra linked via terephthalate linkers to define a three-dimensional ordered network with one-dimensional diamond-shaped channels. One intriguing feature of the MIL-53 family is the dramatically different breathing behavior observed for the different M^{3+} centers. The MIL-53(Cr) solid,[5] for example, exhibits either an orthorhombic *large-pore* (*lp*) form (Figure 1e) – favored by dehydration, higher temperatures and larger adsorbate uptakes – or a monoclinic *narrow-pore* (*np*) form (Figure 1d) found at lower temperatures and lower uptakes.

The iron analogue, MIL-53(Fe), shows a more complex breathing behavior,[12,13] with the dehydrated material adopting a *very-narrow-pore* (*vnp*) form (*C* 2/*c* symmetry) that takes up CO_2 to give an *intermediate* (*int*) staged form before opening sequentially to give the *np* and *lp* forms. Our own studies of the scandium analogue[11,14] indicate a similarly complex, but crystallographically distinct breathing behavior in response to solvent removal, temperature variation and adsorption of H_2O and CO_2. Upon removal of solvent dimethylformamide (DMF) occluded in the as-prepared form, the MIL-53(Sc) does not open but instead contracts to give a *closed-pore* (*cp*) form (*P* $2_1/c$ symmetry) distinct from the *vnp* form (Figures 1a and b) and without accessible porosity to N_2 or CO_2. The solid remains in the *cp* form between 100 and 573 K with a gradual expansion in the unit cell volume in response to increasing temperature, followed by a transition at 623 K to a *vnp* form with *C* 2/*c* symmetry which is isostructural to MIL-53(Fe)-*vnp*.[13] The transition complexity of MIL-53(Sc) goes beyond this sensitive response to temperature variation. Hydrating MIL-53(Sc)-*cp* at room temperature, for example, leads to MIL-53(Sc)-H_2O in the so-called *intermediate* (*int*) phase (in triclinic symmetry; Figure 1c) where half of the channels are partially open due to the uptake of water molecules while the others are empty and closed.[11] The carbon dioxide adsorption isotherm of MIL-

53(Sc)[11,14] is different from that reported for MIL-53(Cr) or MIL-53(Fe). An initial region of zero uptake is followed by two steps: the first at 2 – 3 mmol g^{-1} and the second to 13 mmol g^{-1}. The latter was attributed to full opening to the *lp* form (Figure 1e), as observed for various solids of the MIL-53 structure type upon uptake of large amounts of adsorbates.[5,9,15,16] However, no *in situ* diffraction data was available to confirm the presence of the *lp* form or to establish the structure responsible for uptakes from 2 – 3 mmol g^{-1}.

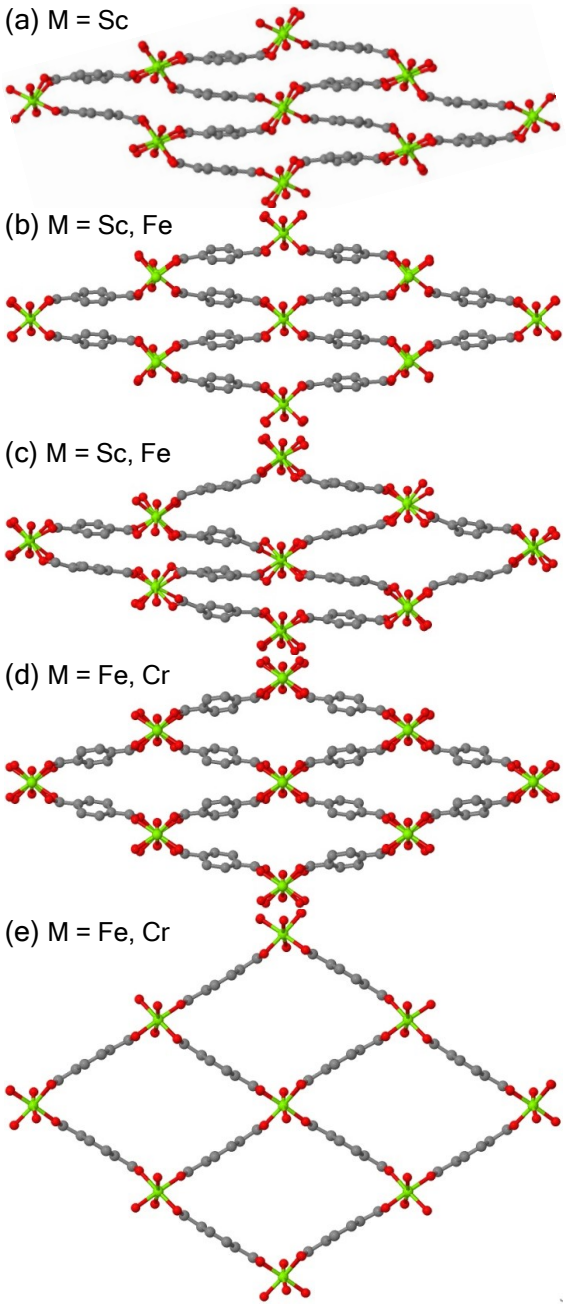

Figure 1. Schematic representation, together with examples, of the different structural forms of MIL-53 observed for different metals: (a), *cp*; (b), *vnp*; (c), *int*; (d), *np*; and (e), *lp*. Color code: gray, carbon; red, oxygen; and green, metal.

A considerable number of multidisciplinary studies have been devoted to understanding the structural transformations observed for breathing MOFs of the MIL-53 type and others.[16-21] In particular, MIL-53(Cr), a textbook example of bi-stable (i.e., *lp* ↔ *np* transition) breathing MOFs, has been extensively explored. Some well-established experimental methods that are routinely deployed include: (1) manometric/gravimetric and microcalorimetric measurements for studying a variety of adsorbate molecules; (2) *in situ* techniques (e.g., X-ray diffraction, infrared or Raman spectroscopy) to, for example, locate adsorbates in the pores or probe the nature of adsorption sites; and (3) quasi-elastic neutron scattering experiments to help understand the dynamics of a probe molecule in a host MOF.[7,22] Hand-in-hand with the experimental effort, theoretical investigations have also been carried out for breathing MOFs on different length and/or time scales.[23-27] The richness of the insights provided by computational methodologies spans from mechanistic details realized through a quantum mechanical (QM) description of the electronic structure of the system[13,28] – primarily relying on static calculations at density functional theory (DFT) level – to macroscopic thermodynamic information on the sample level, which can provide insight into, for instance, the interplay between the adsorbent elasticity and guest molecule adsorption.[27,29] In particular, force field-based molecular simulation studies, both Monte Carlo (MC) and molecular dynamics (MD),[30] have made substantial contributions towards elucidating microscopic mechanisms that govern the structural deformations.[17,21,23,24,31-36]

MD simulation is particularly suited to coupling with experiment to study MOF breathing phenomena by giving a detailed description of the system of interest on the atomic/molecular level. As the simulation results in points in phase space that are connected in time, it can provide an evolving picture for the breathing behavior, which readily conveys valuable details on, for instance, how cooperative movements of the framework ligands, together with the interactions between the inorganic and organic moieties, facilitate the major structural changes of the MIL-53 solids.[3,31] Moreover, information concerning the kinetics and energetics of the breathing can be extracted from MD simulations to help reveal collective effects of the guest-guest, guest-host and sometimes host-host interactions. Up to now, most MD studies present in the literature that aim to capture the breathing phenomena of MOFs made use of tailor-made flexible force fields for the framework. Such force fields are usually arrived at either by employing accurate QM calculations[37] or via a combination of chemical intuition, existing force fields, and an iterative process to tune the parameters to reproduce the experimental data.[23] Despite being very successful in not only reproducing but also helping interpret many structural and dynamical properties of the breathing of MOFs, force field-based MD simulation only has been applied to a handful of selected structures. From a simulation point of view, the lack of suitable force fields and the effort involved in developing a new force field are to blame. These problems may be avoided by using DFT based *ab initio* molecular dynamics (AIMD) simulation techniques (also called DFT-MD or first-principles MD).[38-40] Since finite temperature dynamics is developed with forces obtained directly from first-principles electronic structure calculations, made 'on the fly', AIMD simulations, in principle, allow for an accurate and unbiased investigation of the chemical processes of interest. In addition, they can be more predictive compared to the force-field approach, mainly because pre-defined force fields only can be expected

to reproduce the chemical events against which they are parameterized prior to the simulations. Consequently, AIMD simulations are successfully used in multiple fields of chemistry.[41-45] However, their application to the field of MOFs is still rare.[20,46,47]

In this contribution, we probe and so provide insights into the temperature and CO_2 adsorption-related breathing phenomena of MIL-53(Sc) by means of AIMD simulations and *in situ* synchrotron X-ray powder diffraction (XRPD) experiments. As stated above, MIL-53(Sc) has been studied less than its counterparts MIL-53(Cr) and MIL-53(Fe) and its complex structural transformations, which are different from those of the Cr or Fe version, have yet to be fully measured or understood.[11,14] The MIL-53(Sc) material was therefore an ideal subject for a joint computational AIMD and experimental XRPD study that is the first of its kind. First, we demonstrate a modeling scheme based on AIMD simulation that not only enables a correct prediction of the structural changes of MIL-53(Sc) in response to temperature variation but also provides a molecular-level explanation for them. Then, through a synergic combination of the AIMD simulations and experimental evidence, we determine and elucidate structural transformations upon CO_2 adsorption and in addition explain features of the experimental diffraction pattern that only MD simulations of this type can predict directly.

2. Results and discussion

2.1 Structural Response to Temperature Variation at Zero Guest-Molecule Loading

In a previous work,[14] some of us reported the novel *cp* structural form of MIL-53(Sc) upon removal of the guest molecules. Interestingly, the evacuated structure exhibited unusual thermal behavior. The framework underwent a gradual expansion of the unit cell in response to the increasing temperature until it changed symmetry from $P\,2_1/C$ to $C\,2/c$ at 623 K. The structures obtained at the different temperatures were successfully refined against the XRPD patterns in the same work. Owing to the availability and, more importantly, the subtlety of the structural changes simply caused by varying temperature, these experimental structures provide an ideal test case for critically assessing our computational approach. To mimic the experiments *in silico*, the as-prepared MIL-53(Sc), containing solvent molecules (DMF),[11] was used as the starting configuration for the framework. The DMF molecules were removed from the framework prior to the simulations, analogous to the activation in the experiment. The structure, thereby denoted MIL-53(Sc)-*DMF(removed)*, was then used as a starting structure for AIMD simulations performed at three temperatures, namely 100, 293, and 623 K, which were among the ones investigated experimentally.[14] Note all AIMD-simulated structures reported here were generated by averaging the last portion of the AIMD trajectory (after equilibration), followed by an energy minimization at 0 K in conjunction with the time-averaged cell parameters. Computational procedures used to produce these structures are detailed in the Supporting Information (SI). The simulated cell parameters as well as their standard deviations are given in Table 1, together with the corresponding values from the experiments (in parentheses).[14] For comparison, the starting

configuration for all these AIMD simulations, MIL-53(Sc)-*DMF(removed)*, is also included in Table 1 (in parentheses) to illustrate the significant structural changes between the start and finish of the AIMD simulations. The atomic positions are provided in the SI. Table 1 shows that the agreement between the simulated and experimental unit cells is very good for all the three temperatures investigated (also see Figure S7 in the SI for comparison of the XRPD patterns). The discrepancies are very small and are, in most cases, within the statistical errors. A comparison of selected bond distances and angles between simulation and experiment is given in Table S4 in the SI.

Table 1. Comparison of AIMD-Simulated and Experimental (in Parentheses)[a] Cell Parameters for the *cp* (100 and 293 K) and *vnp* (623 K) forms of MIL-53(Sc)

T (K)	*a* (Å)	*b* (Å)	*c* (Å)	*α* (°)	*β* (°)	*γ* (°)	*V* (Å^3)
100.00	20.22 ± 0.08	7.44 ± 0.04	11.35 ± 0.06	90.00 ± 0.55	103.60 ± 0.52	90.00 ± 0.40	1658.18 ± 7.82
	(*20.30*)	(*7.33*)	(*11.69*)	(*90.00*)	(*104.96*)	(*90.00*)	(*1680.75*)
293.00	20.33 ± 0.14	7.44 ± 0.08	11.48 ± 0.13	90.00 ± 1.15	104.07 ± 1.09	90.00 ± 0.83	1684.89 ± 16.98
	(*20.33*)	(*7.33*)	(*11.84*)	(*90.00*)	(*105.21*)	(*90.00*)	(*1701.36*)
623.00	20.04 ± 0.13	7.42 ± 0.20	13.12 ± 0.15	89.58 ± 3.25	90.25 ± 2.17	90.36 ± 2.39	1950.77 ± 43.39
	(*19.71*)	(*7.27*)	(*13.26*)	(*90.00*)	(*90.00*)	(*90.00*)	(*1901.65*)
starting[b]	(*19.34*)	(*7.30*)	(*18.36*)	(*90.00*)	(*90.00*)	(*90.00*)	(*2593.16*)

[a] Experimental data were taken from the work of Mowat et al.[14]

[b] The experimental MIL-53(Sc)-*DMF(removed)* structure[11] was used as the starting configuration for the simulations at the three temperatures.

In both the experiments and the simulations, remarkable cell volume reductions were observed when removing the DMF molecules from the as-prepared framework; for instance, the structure shrank by as much as 35% at 100 K. Moreover, the AIMD trajectories suggest that structural contractions at all the three temperatures occurred almost immediately after the simulations started, implying that the as-prepared structure with DMF removed is thermodynamically unfavorable. It is also clear, from the standard deviations in Table 1, that considerably larger fluctuations (in the simulated cell parameters) are associated with the structure at 623 K and, on the whole, the higher the temperature, the larger the amplitude of these fluctuations (also see Figure S6 in the SI). This observation is, of course, in accordance with thermodynamic principles.

Besides the gradual expansion of the structure, rotation of the chains of $ScO_4(OH)_2$ octahedra around their long axes in response to increasing temperature was observed both experimentally and computationally for

MIL-53(Sc). The extent of rotation can be quantified using the angle formed between the two planes defined by the two Sc–μ_2-O–Sc groups (shown as dashed lines in Figure 2). This angle is 0 ° in the as-prepared framework structure, MIL-53(Sc)-*DMF(removed)*, the starting configuration for all the three simulations. Experimentally the angles were found to be 36 and 0 ° for the structure at 100 and 623 K, respectively (Figure 2). As it is clearly shown in Figure 2, the AIMD simulations were able to capture almost quantitatively the rotations of the Sc hydroxide chains observed experimentally at the different temperatures, in addition to the accurate reproduction of the cell expansions seen in Table 1. As suggested by these correct predictions of the various MIL-53(Sc) structures, our AIMD simulation-based modeling approach might serve as a means for assisting determination of other forms of MIL-53(Sc) and other MOF structures. Note, the onset of applying the AIMD methodology to a MOF is to establish the capability of chosen DFT functional in describing the system chemistry.[48] Equally important is that the choices of simulation parameters (such as basis set) also need a careful justification (see the SI for method validation in the case of MIL-53(Sc)).

Moreover, it is worth noting that the AIMD simulations yielded the correct MIL-53(Sc) structures at the different temperatures without inputting any prior knowledge of the target structures. This level of predictability cannot be easily achieved by computational approaches based on energy minimization at 0 K. Therefore, these results show that the entropic effects resulting from molecular motion are successfully included in the AIMD approach. Furthermore, the AIMD simulations provided a dynamic picture on the molecular level for helping interpret the cell evolution with increasing temperature. In the AIMD simulations, we observed significantly larger rotational and vibrational movements of the phenyl rings of the terephthalate ligands of the framework at 623 K. Given that the ligand length is almost invariant upon deformation, in order to accommodate these large movements of the phenyl rings, the two Sc hydroxide chains corresponding to the short diagonal of the rhombic cross section of the channel have to move away from each other. At the same time, they continue to rotate until becoming parallel to each other, ultimately resulting in cell expansion and the higher symmetry adopted by the solid at 623 K. Interestingly, despite large movements of the phenyl rings being observed in our simulation at 623 K, no complete "flipping" of the rings has been found for duration of ca. 20 ps (neither at the lower temperatures). Although the time frame may be too short to establish conclusive evidence, our simulations suggest "flipping" be prevented (probably sterically) in less open forms of MIL-53(Sc), which agrees well with our recent ^{2}H NMR data of the solid measured at 400 K.[49]

As a further step to elucidate the structural response of MIL-53(Sc) to temperature variation, energetic information was extracted from the simulations. The potential energies of the three energy-minimized, time-averaged AIMD structures are given in Table 2 together with that of the starting structure (calculation details are provided in the SI). It thus can be confirmed unambiguously that the *cp* structures are indeed energetically favored, corroborating the experimental observations that the solid contracted to adopt the *cp* form upon removal of the guest molecules (water or DMF) from the framework.[11,14] The data in Table 2 also show that

there is a correlation between the framework potential energy and volume, indicating that the structure becomes increasingly energetically unfavorable as it expands.

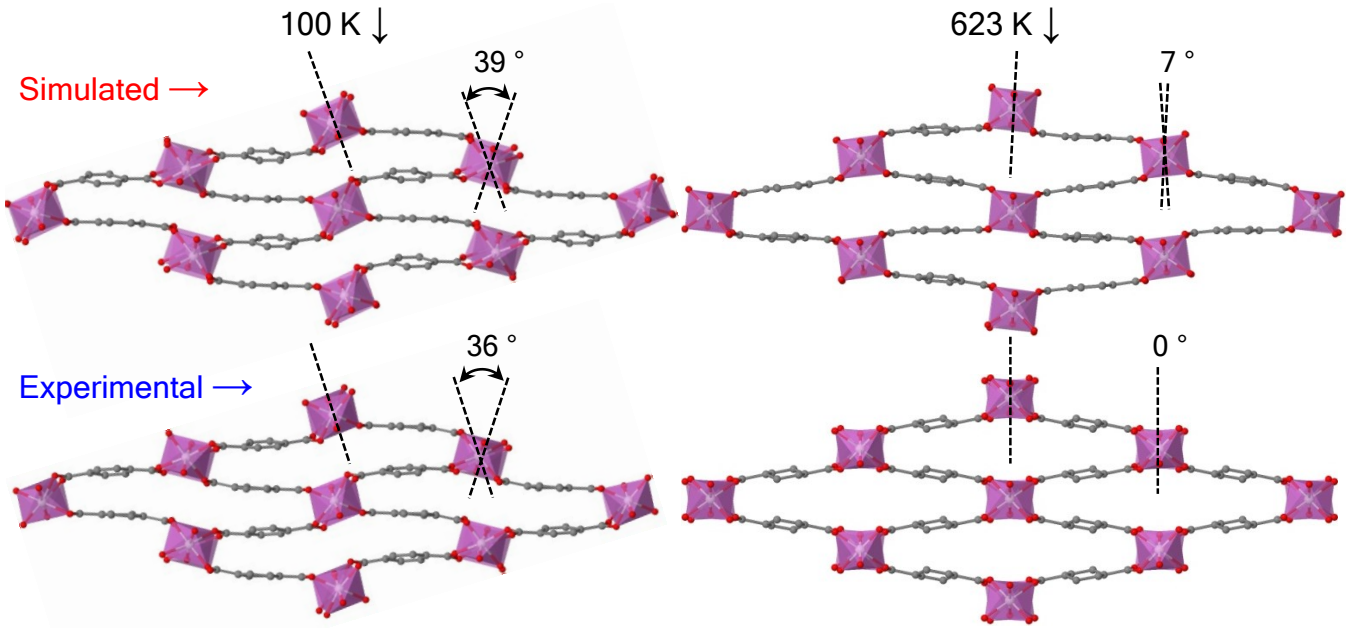

Figure 2. Comparison of the rotation of the Sc hydroxide chains in the AIMD-simulated (upper) and experimental (lower) structures at 100 (left) and 623 (right) K. Dashed line represents the plane of the infinite Sc–μ_2-O–Sc chains. Hydrogen atoms are omitted for clarity.

The influence of dispersion (or van der Waals) interactions on the MIL-53(Sc) structure needs to be emphasized. A complementary AIMD simulation starting with the *cp* structure (obtained at 100 K with dispersion-corrected DFT *a priori*) was performed at 100 K employing only DFT, which is known to account poorly for dispersion interactions.[48,50,51] It was found that the initial *cp* framework gradually opened and the unit cell volume increased by 30% within 3 ps in the AIMD simulation (Figure S8a in the SI), clearly demonstrating that the dispersion interactions play a pivotal role in maintaining the *cp* structure. The herein established understanding of the importance of dispersion interactions in determining the MIL-53(Sc) structure is in good agreement with the literature findings for other flexible MOFs.[20,36,52]

Figure 3 provides a structural basis for understanding the relative stabilities of the *cp* and *vnp* structures as suggested by the energy difference (Table 2). In the *cp* structures (at both 100 and 293 K) the two opposite Sc hydroxide chains corresponding to the short diagonal of the rhombic cross section of the channel are present in an energetically favorable conformation. That is the hydrogen atom of every hydroxyl group interacts strongly with the nearest oxygen atom of the carboxylate group belonging to the opposite chain with the

interatomic distances being 2.05 and 2.15 Å at 100 and 293 K, respectively. In contrast, the formation of such strong and directional hydrogen bonds does not occur in the *vnp* structure, as suggested by the distance between the pair being 3.8 Å, resulting from the different alignment of the chains at 623 K compared to the configurations in the *cp* structures (Figure 3). From this comparison it follows that the predominant hydrogen bonds formed between the two opposite inorganic chains give rise to large intra-framework interactions which in turn results in the *cp* structures being more stable than the *vnp* structure (Table 2). This energetic information complements the dynamic picture of the structural transformations upon the action of temperature obtained from the AIMD trajectories in explaining why the *vnp* structure only can be realized at much higher temperatures. The larger variations and rotations within the framework (larger kinetic energies) resulting from the higher temperature help to overcome the strong intra-framework interactions present in the *cp* form and eventually stabilize the structure in a relatively high potential energy configuration (i.e., *vnp*).

Table 2. Calculated Potential Energies for the Various MIL-53(Sc) Framework Structures[a]

MIL-53(Sc)-*i*	ΔE (kJ mol^{-1})	ΔV (Å^3)
cp(100 K)	0.0	0.0
cp(293 K)	3.4	26.7
vnp(623 K)	194.6	292.6
DMF(removed)	359.6	935.0

[a] Potential energy (ΔE) and volume (ΔV) per MIL-53(Sc) framework consisting of 8 $ScO_4(OH)_2$ units. Both values are reported for the particular framework with respect to those of the MIL-53(Sc)-*cp* structure simulated at 100 K. Note all energies were determined by single-point calculations where the same exchange-correlation grid (constant density of grid-points) was used.

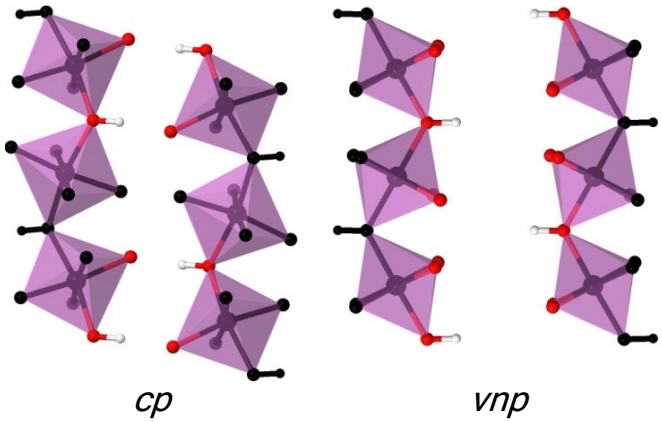

Figure 3. Illustration of the different conformations of the two opposite Sc hydroxide chains in the *cp* and *vnp* forms of MIL-53(Sc). The hydroxyl groups in the central channel, together with their nearest oxygen atoms of the carboxylate groups belonging to the opposite chain, are color coded: white, hydrogen; and red, oxygen.

2.2 Structural Response to CO_2 Adsorption at 196 K

Adsorption isotherm and *in situ* XRPD patterns

The CO_2 adsorption behavior of dehydrated MIL-53(Sc) at 196 K, reported previously,[11] is shown in Figure 4a. In the adsorption branch of the isotherm, negligible amounts of CO_2 are adsorbed up to 0.05 bar. After that, a first step with adsorption of around 2 – 3 mmol g^{-1} is observed, followed by a second step (starting at ca. 0.75 bar) to an uptake of around 13 mmol g^{-1}. The *in situ* XRPD patterns collected on the MIL-53(Sc) sample during the CO_2 adsorption at 196 K (Figure 4b) show a remarkable phase evolution of the structure as a function of the CO_2 pressure. The initial structure after outgassing is the *cp* form, which has no apparent porosity to accommodate any measurable amount of CO_2. This is evident from both the adsorption isotherm and the pattern collected at 0.03 bar, which is largely identical to the one collected on the starting, evacuated solid. As the partial pressure of CO_2 is increased, characteristic XRPD peaks appear at the same pressure regions where the steps in the adsorption isotherm can be observed, displaying a clear correlation between the structural transformations and the amounts of CO_2 adsorbed. At 0.148 bar, corresponding to the beginning of the first plateau in the adsorption branch, a new XRPD signature can be observed and it continues to be distinguishable up to higher pressures. The uptake of 2 – 3 mmol g^{-1} might be accommodated by either an *int* form where one-half of the channels are partially open and the others are closed (Figure 1c) or by a *np* form where all channels are partially open (Figure 1d). Note that both forms are observed for MIL-53(Fe) with CO_2 adsorbed.[13] Further investigations were conducted to determine the structural form and are discussed in detail below. After this initial period of low uptake (ca. 2 – 3 mmol g^{-1}), the second step happens in a much narrower pressure region and the complete filling of the pores leads to a new structural phase as suggested by the XRPD patterns at the high pressures. However, the existence of the high-pressure form is notably in mixture with the other forms observed at the lower pressures. The coexistence of multiple crystallites is similar to the previously reported structures of MIL-53(Fe) upon adsorption of (C2 – C4) alkanes.[16] Interestingly, although the XRPD patterns show reversible phase transitions upon desorption, the structure observed at the first plateau of the adsorption isotherm rather than the *cp* form was retained in the final, outgassed solid. This somewhat surprising result suggests longer evacuation time (and possibly a more aggressive procedure) may be needed to fully re-activate the solid.

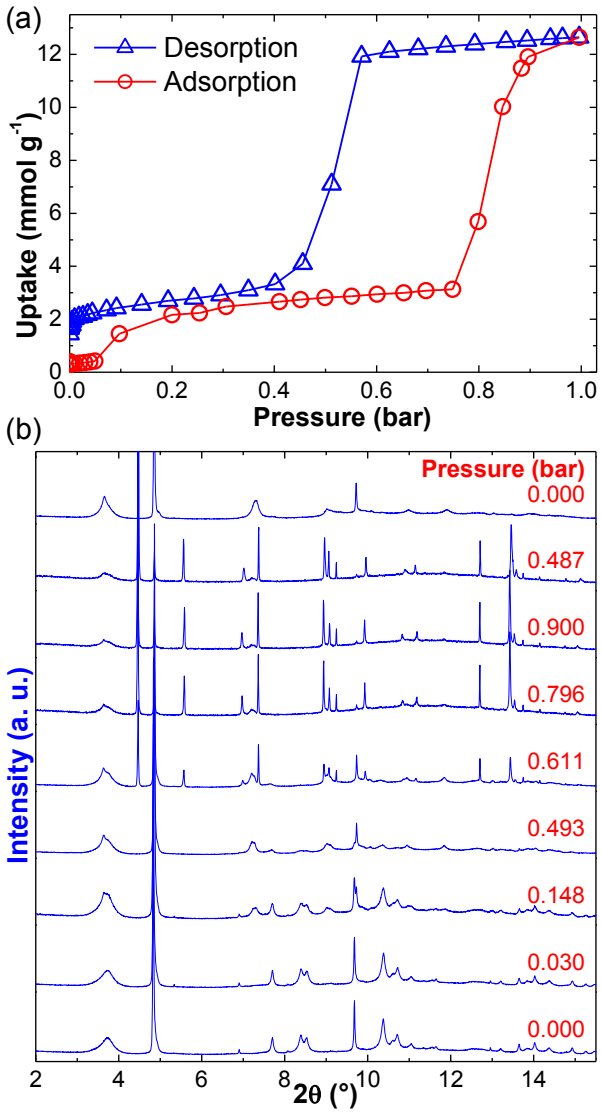

Figure 4. Adsorption of CO_2 on dehydrated MIL-53(Sc) at 196 K followed by XRPD: (a) adsorption and desorption isotherms of CO_2; and (b) variation of the XRPD patterns with the CO_2 pressure.

MIL-53(Sc) structure at low CO_2 loadings

Unambiguous indexing of the pattern at 0.493 bar CO_2 pressure proved unsuccessful due to the significant peak broadening in the experimental pattern (Figure 4b). Since the patterns at higher loadings show clear evidence for the high-pressure form as a highly crystalline phase, there is no indication that the broadening was a result of beam damage or other degradation, rather a structural feature associated with a lowering of symmetry. Rietveld refinement using starting literature models, including those of MIL-53(Sc), could not be performed, as the ambiguity in the unit cell and the broadened features of the experimental pattern preclude a suitable model for refinement. On the other hand, conventional computational approaches based on energy minimization could not be used to assist the structure determination, since they rely on the prior knowledge of

both cell parameters and starting configuration for the target structure.[13,53,54] Here, we circumvented these restrictions by means of the AIMD simulation approach that has already demonstrated the excellent prediction of the structural changes in response to temperature variation. Again, the MIL-53(Sc)-*DMF(removed)* structure was used as the starting configuration for the framework while the initial CO_2 positions were generated by grand-canonical Monte Carlo (GCMC) simulations (details are given in the SI).[30] As MIL-53(Sc) exhibits the *cp* form after activation, from a simulation standpoint two scenarios regarding the pore-opening mechanism exist. That is the CO_2 adsorption occurs in either only half or all of the channels, leading to the *int* or *np* topology, respectively. No conclusive evidence could be established at this stage to verify these structural assignments. Therefore, both hypotheses were tested computationally in parallel (details are given in the SI). The final energy-minimized, time-averaged AIMD structure for the MIL-53(Sc)-*int* form has a triclinic setting (space group *P* 1) with simulated lattice parameters of $a = 20.658 \pm 0.152$ Å, $b = 21.211 \pm 0.170$ Å, $c = 7.413 \pm 0.093$ Å, $\alpha = 92.055 \pm 0.830$ °, $\beta = 88.335 \pm 0.547$ °, and $\gamma = 38.051 \pm 0.445$ °. The topology of the *int* phase is characterized by two sets of diamond-shaped channels of different pore size (open and closed), doubling the number of atoms in the unit cell of the as-prepared structure (Figure 5a). The structure corresponding to the *np* topology is discussed in detail in the SI.

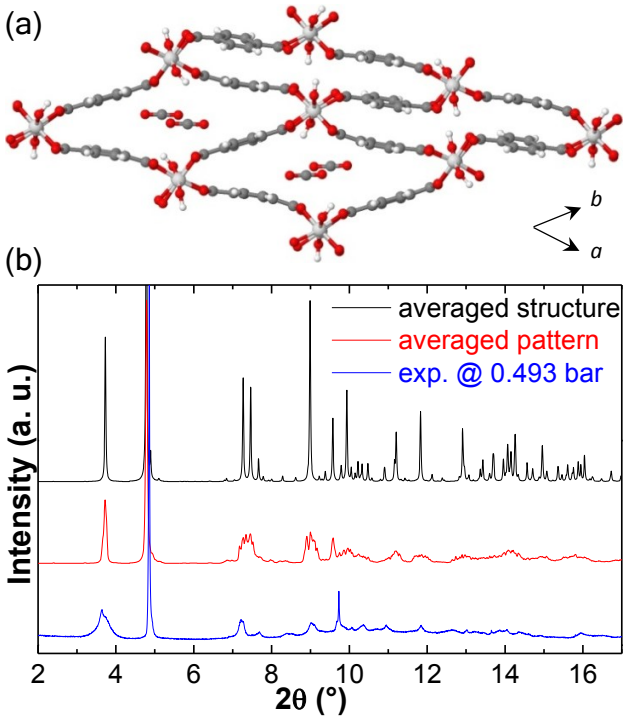

Figure 5. AIMD-simulated MIL-53(Sc)-*int* structure for a CO_2 loading of 2.2 mmol g^{-1}. (a) Unit cell viewed down the channel direction. (b) Comparison of the experimental XRPD pattern collected at 0.493 bar CO_2 pressure with two simulated patterns. One (in black) was calculated on the energy-minimized, time-averaged AIMD structure (illustrated in Figure 5a), while the other (in red) was generated by averaging over a series of patterns based on the snapshot structures (of the same AIMD trajectory used to obtain the time-averaged structure).

First, it is clear from Figure 5b that the experimental XRPD pattern corresponding to the first plateau of the CO_2 adsorption isotherm compares well to the simulated pattern based on the *int* structure, thus confirming MIL-53(Sc) adopts this form rather than the *np* form (the corresponding comparison of XRPD pattern is shown in Figure S10 in the SI). Furthermore, the *int* phase can be clearly identified in the experimental patterns for pressures ranging from 0.148 to 0.900 bar and during the evacuation (Figure 4b). This *int* form induced by adsorbing CO_2 in only one-half of its channels (Figure 5a) is, as expected, similar to the hydrated MIL-53(Sc) and the MIL-53(Fe)-*int* structure (but differing in crystallographic detail). It should be noted that the MIL-53(Sc)-*int* structure is stable during CO_2 adsorption, as opposed to the metastable MIL-53(Fe)-*int* structure or the soft mode observed in the Cr solid.[12,16,24] Remarkably, the AIMD simulation suggests a possible explanation for the strong and anisotropic broadening of the experimental XRPD peaks, which hindered the application of more conventional approaches to solving the structure. Figure 5b shows that the pattern on the averaged structure (i.e., the energy-minimized, time-averaged *int* structure illustrated in Figure 5a) gives all the characteristic peaks that are observed in the experimental pattern, but the peaks are too narrow, even though the broadening used in the pattern simulation was that observed for the same sample, at the same temperature, but in the *lp* form at higher values of partial pressure of CO_2. Averaging a series of patterns (the individual patterns are shown in Figure S9 in the SI) based on the snapshots taken during the AIMD simulation yielded an even better agreement with the experimental pattern. Therefore, the anisotropically-broadened features of the experimental patterns may be interpreted as a result of the motion and disorder of the adsorbent-adsorbate structure that is identified by the AIMD simulation. While the (***) and (***) reflections, at 4.9 ° and 9.8 ° 2θ, are sharp in experimental and simulated patterns, most other reflections are strongly broadened in the experimental pattern, as predicted by the simulation. In summary, framework dynamics, often causing a loss of long-range order and hence broad peak shape, has been shown to make structure determination difficult by diffraction on its own.[21,55] Here, the averaged pattern is effectively a more realistic representation of the thermally disordered macroscopic sample, thus in better agreement with the experimental XRPD pattern. On the other hand, the averaged structure is an idealized model that is more "crystalline" than the experimental sample, displaying narrower and sharper peaks. The greater degree of order compared to experiment is clearly a result of the artificial periodicity induced by the combination of finite simulation cell and periodic boundary conditions imposed.

A close inspection of the conformations of the CO_2 molecules located in the open channels of the *int* structure reveals the microscopic adsorption mechanism. Figure 5a shows that the CO_2 molecules are aligned with the long diagonal of the rhombic cross section of the channel and are positioned at the center of the pores, interacting strongly with the hydroxyl groups of the two opposite Sc hydroxide chains corresponding to the short diagonal of the rhombus shape. The CO_2 molecules are closely 'stacked' along the channel and are almost parallel to each other, forming a zigzag-like chain of CO_2 along the channel direction as illustrated in Figure 6a. Every CO_2 molecule is slightly tilted and displaced to favor a conformation where the oxygen atom of each CO_2 molecule 'pulls' the carbon atom of a neighboring CO_2 molecule.

The radial distribution functions (RDFs)[56] were utilized to characterize time-resolved conformational changes of the adsorbed CO_2 molecule with respect to other CO_2 molecules and the framework (Figure 6c). The characteristic distance between the carbon atoms of two adjacent CO_2 molecules, $C(CO_2)\cdots C(CO_2')$, is 3.65 Å, measured by the first distinct peak of the RDF for the pair. Likewise, the RDF plotted for the $C(CO_2)\cdots O(CO_2')$ pair confirms the close proximity by displaying the first peak centered at 3.30 Å. These short distances between adjacent CO_2 molecules along the channel give rise to strong CO_2-CO_2 interactions. These observations from our AIMD simulations are in line with the joint experimental and theoretical investigation of CO_2 adsorption in MIL-53(Cr) reported previously.[31] However, the distances between neighboring CO_2 molecules in MIL-53(Sc) are larger than the ones observed in the case of MIL-53(Cr), wherein $C(CO_2)\cdots C(CO_2')$ and $C(CO_2)\cdots O(CO_2')$ were 3.40 and 3.15 Å, respectively. This might be explained partly by the larger *c* dimension of the MIL-53(Sc) unit cell resulting from the larger ionic radius of Sc^{3+}.

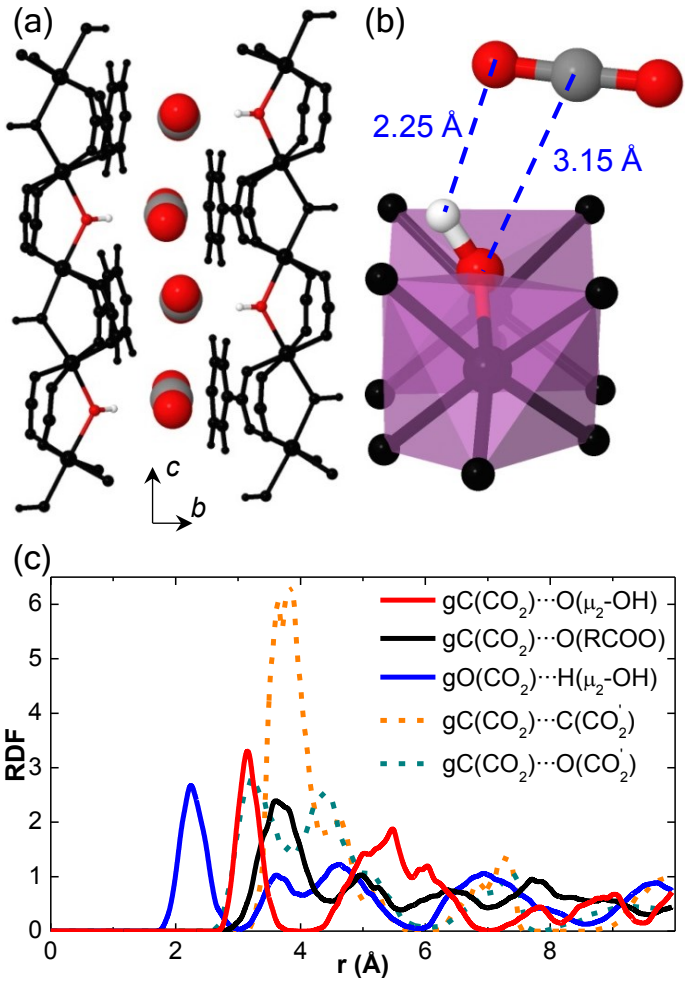

Figure 6. AIMD-simulated MIL-53(Sc)-*int* structure for a CO_2 loading of 2.2 mmol g^{-1}. View of the partially open channels (a) and double-interaction between CO_2 and hydroxyl group of the framework (b); where the

CO_2 molecules and hydroxyl groups are color coded: white, hydrogen; gray, carbon; and red, oxygen. (c) Radial distribution functions computed over the last 10 ps of the AIMD simulation.

More significantly, our AIMD simulations show the formation of electron donor-acceptor (EDA) complexes between the CO_2 molecules and the framework. As illustrated in Figure 6a, each adsorbed CO_2 molecule is situated in close proximity of a hydroxyl group. The CO_2 and hydroxyl group are 'bridged' by a double interaction (Figure 6b), i.e., the $C(CO_2)\cdots O(\mu_2\text{-OH})$ and $O(CO_2)\cdots H(\mu_2\text{-OH})$ interactions, which can be confirmed by the corresponding RDFs where characteristic peaks are centered at 3.15 and 2.25 Å, respectively. Moreover, the fact that the $C(CO_2)\cdots O(\mu_2\text{-OH})$ distance (3.15 Å) is shorter than the $C(CO_2)\cdots O(RCOO)$ distance (3.55 Å) demonstrates that the carbon atom of the CO_2 molecule interacts preferentially with the oxygen atom of the hydroxyl group over that of the carboxylate group of the framework. In other words, the EDA complex is formed between the $C(CO_2)$ acting as the electron acceptor and the $O(\mu_2\text{-OH})$ acting as the electron donor. Our AIMD simulations thus provided a first evidence for the nature of the strong CO_2-framework interactions in the MIL-53(Sc)-*int* structure. The CO_2 location, relative to the hydroxyl group of the framework, deduced from our AIMD simulation (Figure 6) is in good agreement with several literature findings. That is, similar $C(CO_2)\cdots O(\mu_2\text{-OH})$ EDA complexes have been reported for CO_2 adsorption in MIL-53(Cr) and non-functionalized MIL-53(Fe).[13,31,57] However, further experimental investigations such as infrared spectroscopic measurements are necessary to judge the accuracy of this modeling prediction.[57] The strong CO_2-CO_2 interactions present in the *int* structure are essential for facilitating the observed $C(CO_2)\cdots O(\mu_2\text{-OH})$ EDA complexes (see further discussion in the SI). This EDA-related phenomenon has been explored by several DFT studies in various MIL-53 solids.[13,31] In those studies, the CO_2 molecule was typically placed inside the framework initially by the simulator. The different CO_2 configurations relative to the framework were then examined by the energy minimization calculations at 0 K, in which, however, one normally would not expect to see dramatic steric changes. In contrast, our simulations arrived at the final configurations starting from a completely different picture, as clearly demonstrated by the structural evolution of MIL-53(Sc)-*int* during the course of the AIMD simulation given in the SI. In passing, we note that the dispersion interactions again were found to be crucial for stabilizing the *int* structure. It can be seen in Figure S8b (in the SI) that the volume of the CO_2-loaded framework increased by more than 60% within 3 ps in the AIMD simulation where dispersion corrections were not applied to the DFT calculations.

MIL-53(Sc) structure at high CO_2 loadings

The structural phase observed at the high CO_2 pressures (0.611 – 0.900 bar) was also determined by AIMD simulations as described in the SI. The final energy-minimized, time-averaged MIL-53(Sc)-*lp* structure has an orthorhombic unit cell with lattice parameters of a = 7.354 ± 0.100 Å, b = 17.155 ± 0.112 Å, c = 13.442 ± 0.068 Å, α = 90.000 ± 0.580 °, β = 90.000 ± 0.561 °, and γ = 90.000 ± 0.546 °, in very good agreement with

the experimentally indexed orthorhombic *Imma* cell with parameters of a = 7.310(1) Å, b = 17.029(2) Å, and c = 13.504(1) Å.

In parallel, since the lattice parameters of the *lp* structure were known from the experiment, we used them to identify the atomic positions of the framework atoms applying a procedure based on molecular energy minimization calculations explained previously.[58-60] Thereafter, we included and optimized the positions of the adsorbed CO_2 molecules using GCMC simulations (full details are given in the SI). Figure 7 compares the experimental XRPD pattern collected at 0.900 bar CO_2 pressure with simulated patterns based on the two computationally anticipated structures (models 1 and 2). Both modeling approaches, i.e., the AIMD simulation and the energy minimization in conjunction with the experimental unit cell, were able to assist structure determination of the *lp* phase. While the energy minimization-based approach is computationally much less expensive and is therefore the obvious choice when the cell parameters are known experimentally, the computationally more expensive AIMD is the only viable option if the experimental cell parameters are not known *a priori*.

The AIMD simulations indicate that 16 CO_2 molecules can be accommodated per unit cell of the *lp* structure while the maximum uptake observed experimentally is around 13 mmol g^{-1} (corresponding to ca. 12 CO_2 per unit cell). This suggests that a fraction of the pores in the solid remain closed even at this high uptake in line with the *in situ* XRPD measurements (Figure 4b) which suggest the coexistence of *int* and *lp* phases. It can thus be concluded that during CO_2 adsorption two structural transformations occur, i.e., *cp* → *int* → *lp*, and MIL-53(Sc) adopts a mixture of two phases over a wide range of pressure, probably due to kinetic restrictions.

In contrast to the clear establishment of $C(CO_2)\cdots O(\mu_2\text{-}OH)$ EDA complexes – where the CO_2 molecule is strongly "anchored" by the hydroxyl group – in the AIMD simulation of the *int* form (Figure 6), the situation in the *lp* form is markedly different. The *lp* simulation indicates $C(CO_2)$ no longer exclusively interacts with $O(\mu_2\text{-}OH)$, but rather shows more frequent preferential arrangements with O(RCOO). In addition, the interatomic distances of the pairs defined in Figure 6c are consistently smaller compared to the ones in the *int* form, due to the condensation of CO_2 in the pores at this high loading (16 CO_2 per unit cell). These observations are in line with the findings made for adsorption of small gas molecules in the *lp* MIL-53(Cr) or MIL-47 solids.[33,35,61,62]

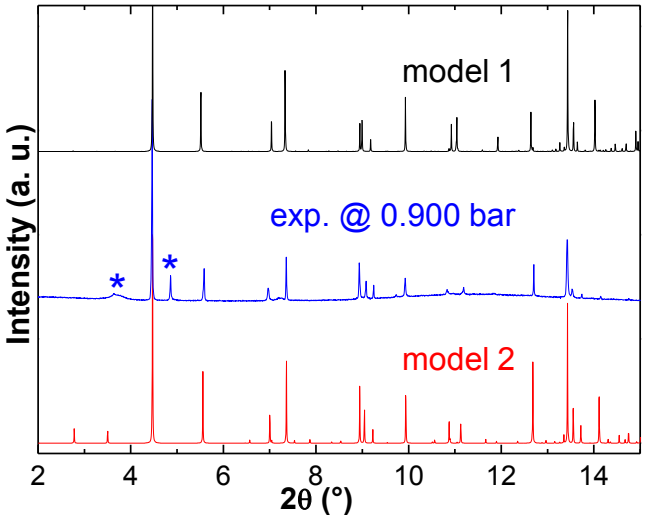

Figure 7. Comparison of the experimental pattern collected at 0.900 bar CO_2 pressure with two computational *lp* models: 1 was realized by AIMD simulations and 2 was generated through a combination of GCMC simulations and energy minimizations in conjunction with the experimental unit cell. Diffraction peaks marked with (*) indicate residual MIL-53(Sc)-*int* and were excluded when fitting MIL-53(Sc)-*lp* and comparing simulated patterns. Model 2 yields a better agreement with the experimental pattern, as the R_{wp} values are ~10% and ~8% for models 1 and 2, respectively.

Energetics of the different forms and structural transformations

Further fundamental insight into the different structural forms of MIL-53(Sc) upon CO_2 adsorption can be obtained by analyzing the potential energy of the framework structures and pore-opening energy of the structural transformations. Table 3 summarizes the potential energy determined for each empty framework, i.e., the CO_2 molecules were not included in the calculations (computational details can be found in the SI). Combining the potential energies of the *vnp* and DMF-removed, as-prepared frameworks reported in Table 2, it is clear that the *cp* structures are indeed the global minimum for a given temperature, because the energy of any other form is positive with respect to that of the *cp* form. It can also be seen that the more open the structure is, the more energetically unfavorable it becomes (Tables 2 and 3). This decreasing structural stability with the expanding framework can be largely attributed to the decrease of dispersion in the lesser and lesser dense structure (see Figure S13 in the SI). The only outlier is the *int* structure which is more stable than the *vnp* structure regardless of having a larger cell volume. This can be rationalized by the fact that the *int* structure has one-half of its channels remaining in the *cp* form which has a much lower energy than the *vnp* form.

It should be emphasized that the calculated potential energy of the various forms of MIL-53(Sc) is the internal energy (at 0 K) of the particular framework configuration induced by either the increasing temperature or the

CO_2 adsorption. That is this energetic information can be indicative of the relative stability of the different empty framework structures but does not necessarily convey speculation on the actual structural transformation in response to an external stimulus. To be specific, in the absence of guest molecules, increasing the temperature converts the *cp* to the *vnp* and not the *int*, although this might be counter-intuitive if solely taking into account the potential energy differences between the three forms. The reason why the *vnp* form rather than the *int* form is adopted by the solid at 623 K is that the large kinetic energy due to the high temperature acts on the whole framework rather than only part of it. This means that the empty *int* framework cannot be maintained at 623 K because the closed half of the structure would restrict large motions which are inevitable at this high temperature. This is in essence the same as the fact that the *vnp* form is observed in place of the *cp* form at 623 K, even though the *cp* phase has the lower potential energy.

The relative stabilities of the various structural forms indicated by the energy differences thus allow us to interpret the different breathing behaviors of the MIL-53 solids upon evacuation from an energetic perspective. Removing guest molecules from the MIL-53(Sc) framework always results in the *cp* structure, because it is the most energetically favored. In contrast, outgassed MIL-53(Cr) adopts the *lp* phase, in line with a previous theoretical study in which the dehydrated *lp* structure was found to be lower in energy than its *np* counterpart.[28]

Table 3. Potential Energies for the Empty MIL-53(Sc) Structures and Pore-Opening Energies for the Different Structural Transformations

MIL-53(Sc)-*i*	ΔE^a (kJ mol^{-1})	ΔV^a (Å^3)
cp	0.0	0.0
int[b]	146.6	334.1
np[b]	318.9	661.6
lp[b]	644.5	1733.5
pore-opening energy[c] (kJ mol^{-1})		
cp(0.0) → *int*(2.2)		-77.3
cp(0.0) → *np*(2.2)		+95.8
int(2.2) → *int*(3.3)		-57.7
int(2.2) → *np*(3.3)		+89.6

[a] Framework potential energy (ΔE) and volume (ΔV) per 8 $ScO_4(OH)_2$ units relative to those of the *cp* structure simulated at 100 K.

[b] Prior to calculation CO_2 molecules were remove.

[c] Energy required for the particular structural transformation. The framework topology is given in *italic* and the CO_2 loading in mmol g^{-1} is given in parentheses

Note all energies were determined by single-point calculations where the same exchange-correlation grid (constant density of grid-points) was used.

Given a particular amount of CO_2 adsorbed, the energy required for different structural transformations to accommodate the uptake was determined to elucidate the phase evolution in response to CO_2 adsorption (Table 3). As a first approximation, the sorption-induced pore-opening energy can be estimated from the energy difference before and after uptake of a certain amount of CO_2 (calculation details can be found in the SI). The energy needed to open the *cp* structure to form the *int* or *np* topology is -77.3 or +95.8 kJ mol^{-1}, respectively. The negative pore-opening energy confirms that the *int* structure can be expected to be formed as a result of exposure of the MIL-53(Sc)-*cp* to CO_2. In contrast, the large positive value in the case of the *np* structure entails the need for a significant amount of external energy to initiate the pore opening thus providing further evidence that in the experiment only the *int* structure is formed. To ascertain the preferential structural transformation for further CO_2 adsorption starting from the *int* structure with a loading of 2.2 mmol g^{-1} (4 CO_2 per unit cell of the *int* structure), we proceeded to consider a higher uptake of 3.3 mmol g^{-1} (6 CO_2 per unit cell of the *int* structure). Two scenarios were investigated: (1) the additional CO_2 adsorption occurred in the already open channels, thus maintaining the *int* topology; and (2) the initially closed channels were opened due to the uptake, leading to a *np* topology. A schematic representation of the two structural transformations can be found in Figure S4 in the SI. The pore-opening energies were found to be -57.7 and +89.6 kJ mol^{-1} for the *int*(2.2) → *int*(3.3) and *int*(2.2) → *np*(3.3) transformations, respectively. This indicates that upon CO_2 adsorption the MIL-53(Sc) solid favors saturating the open channels over initiating new openings of the closed ones, corroborating the *in situ* XRPD patterns which suggest the presence of the *int* phase up to high CO_2 partial pressures.

3. Conclusions

The breathing behavior of the MIL-53(Sc) solid in response to temperature variation and CO_2 adsorption was probed and elucidated through a joint experimental and computational investigation. The AIMD simulation-based approach was first demonstrated to predict accurately the *cp* and *vnp* forms of MIL-53(Sc) at the different temperatures. With the increasing temperature, not only were the cell expansions quantitatively predicted but the subtle differences between the rotations of the Sc hydroxide chains were also correctly captured. Combining the same modeling approach with the *in situ* XRPD experiments, the structural transformations of MIL-53(Sc) upon the CO_2 adsorption were studied. The significantly broadened XRPD peaks of the phase at 0.493 bar CO_2 pressure posed a hurdle to structure determination by commonly adopted methods such as Rietveld refinement or energy minimization. We therefore carried out AIMD simulations that allowed the solvent-removed, as-prepared framework with the CO_2 loadings of interest to evolve freely at the experimental temperature. The simulations successfully facilitated the determination of the MIL-53(Sc)-*int* structure for the phase (at 0.493 bar) corresponding to the first plateau of the CO_2 adsorption isotherm (ca. 2 – 3 mmol g^{-1}). While AIMD simulations were the only viable choice to identify the *int* structure, the *lp* phase with the unit cell indexed experimentally was successfully solved by both the AIMD and energy

minimization-based approaches. The latter is of course more computationally efficient and, therefore, should be used to predict atomic positions of the structure when the cell parameters are available.

Apart from assisting the structure determinations, the AIMD simulations further provided the molecular-level dynamic and energetic information that helped to reveal the nature of the structural responses of MIL-53(Sc) to the external stimuli. The dynamical properties of the system as suggested by the corresponding AIMD trajectory were successfully used to explain, for example, the higher symmetry adopted by the solid at 623 K and the EDA complex formed between the CO_2 molecule and the framework. Equally insightful was the energetic information extracted from the AIMD simulations. The calculated framework potential energies provided an indication of the relative stability of the various identified structural forms, while the calculated pore-opening energies helped to interpret the experimentally observed phase transitions upon CO_2 adsorption.

This work is to the best of our knowledge the first systematic demonstration of applying AIMD simulations to studying the flexibility of MOFs upon temperature variation and adsorption uptake. A special focus was on showcasing the applicability of the methodology to assisting structure determinations when the more conventional techniques failed. Since the energies and forces are calculated by chosen QM method 'on the fly', AIMD simulations are likely to permit investigation of a larger number of flexible MOFs computationally than force field-based approaches. For example, the effects of the nature of the metal on the breathing of the MIL-53 solids with different metals have not yet been fully understood or pursued in parallel by MD simulations. On the basis of reproducing correctly the different breathing behaviors by AIMD simulations, the first-principles descriptions of the MIL-53 variants obtained from those simulations might help to diminish the knowledge gaps in our understanding of the phenomena. Last but not least, as demonstrated by the successful identification of the MIL-53(Sc)-*int* structure in this work, AIMD simulations can be really predictive and are certainly worth exploring in a wider context in the field of MOFs and other flexible and dynamic microporous solids.

4. Methods

4.1 Experimental Details

The MIL-53(Sc) sample used for the *in-situ* measurements was prepared via the reported method.[11] A typical reaction for the preparation of MIL-53 was prepared using a solution of scandium nitrate hydrate, terephthalic acid, pyridine and N,N-dimethylformamide in a molar ratio ($Sc(NO_3)_3 \cdot 3H_2O$) : H_2BDC : C_5H_5N : DMF of 1 : 1 : 15 : 200. The solution was then thoroughly mixed by stirring at room temperature and heated at 463K for 40 hours in a Teflon lined stainless-steel PARR autoclave. Following the reaction, samples were filtered and washed thoroughly with either DMF or ethanol and dried in a drying oven at 323 K. In preparation for the gas loading measurements, samples were ground and packed into 0.7 mm quartz capillaries and a glass wool plug

was inserted to prevent the powder from moving upon evacuation. The capillary was attached to a goniometer head with an attached gas line allowing connection to the pressure control board and turbo pump. Samples of MIL-53(Sc) were activated at 623 K for 10 hours in a tube furnace prior to the experiment and again at 373 K under evacuation with the turbo pump to ensure complete removal of guest species from within the pores. Gas was manually dosed into the system in small increments and the exact pressure was recorded from the attached gauge. The pressure steps selected were based on the adsorption isotherm to gain *in-situ* data for all the structural forms predicted to occur over the course of the CO_2 isotherm, i.e., the *closed-pore* structure upon activation, an *intermediate* structure from ca. 0.2 – 0.7 bar, and the fully loaded form (MIL-53(Sc)-*lp*). Data were collected at Diamond Light Source beamline I-11 using a position-sensitive detector (PSD) comprising 18 MYTHEN-II detector modules covering the angular range of 0 – 90 ° 2 θ with an angular resolution of 0.005 °. Due to the small gap between detector modules, two datasets were collected 0.25 ° apart and the data were merged to give a continuous dataset. The datasets presented here and used in the Rietveld refinement were merged from two 8 second data collections which allowed for rapid *in-situ* monitoring of the evacuation, dehydration and adsorption processes to ensure observed changes were completed before continuing.

4.2 Computer Simulations

All AIMD simulations and DFT-based geometry optimization calculations were performed employing DFT (with periodic boundary conditions and *P* 1 symmetry) as implemented in the QUICKSTEP[63] module of the CP2K[56] simulation package. Energies and forces were calculated with the Gaussian plane wave scheme[63,64] which uses a dual basis set method. This is that a linear combination of Gaussian-type orbitals is used to describe the Kohn-Sham molecular orbitals while the electron density is described by an auxiliary plane-wave basis set. A double-ζ valence plus polarization basis set, in conjunction with the relativistic, norm-conserving Goedecker-Teter-Hutter pseudopotentials, was used for all elements other than Sc, which was described by the MOLOPT basis set.[65-68] All calculations were done using the Becke-Lee-Yang-Parr (BLYP)[69,70] exchange-correlation functional with semiempirical dispersion corrections to the energies and gradients from the DFT-D3[71] method, unless explicitly stated otherwise. Born-Oppenheimer MD simulations were carried out in the isobaric-isothermal ensemble (NPT; constant number of particles, pressure, and temperature). Note that in all the AIMD simulations carried out in this contribution both the shape and dimensions of the simulation box could vary and no constraints were applied to any degree of freedom of the system. Extensive computational details on the calculation setup and modeling procedures can be found in the SI.

Notes and references

‡The authors declare no competing financial interest.

[1] Zhou, H.-C.; Long, J. R.; Yaghi, O. M. *Chem. Rev.* **2012**, *112*, 673.

[2] Kitagawa, S.; Kitaura, R.; Noro, S.-i. *Angew. Chem. Int. Ed.* **2004**, *43*, 2334.

[3] Ferey, G.; Serre, C. *Chem. Soc. Rev.* **2009**, *38*, 1380.

[4] Horike, S.; Shimomura, S.; Kitagawa, S. *Nat Chem* **2009**, *1*, 695.

[5] Serre, C.; Millange, F.; Thouvenot, C.; Noguès, M.; Marsolier, G.; Louër, D.; Férey, G. *J. Am. Chem. Soc.* **2002**, *124*, 13519.

[6] Serre, C.; Mellot-Draznieks, C.; Surblé, S.; Audebrand, N.; Filinchuk, Y.; Férey, G. *Science* **2007**, *315*, 1828.

[7] Ferey, G.; Serre, C.; Devic, T.; Maurin, G.; Jobic, H.; Llewellyn, P. L.; De Weireld, G.; Vimont, A.; Daturi, M.; Chang, J.-S. *Chem. Soc. Rev.* **2011**, *40*, 550.

[8] Horcajada, P.; Gref, R.; Baati, T.; Allan, P. K.; Maurin, G.; Couvreur, P.; Férey, G.; Morris, R. E.; Serre, C. *Chem. Rev.* **2011**, *112*, 1232.

[9] Loiseau, T.; Serre, C.; Huguenard, C.; Fink, G.; Taulelle, F.; Henry, M.; Bataille, T.; Férey, G. *Chem. – Eur. J.* **2004**, *10*, 1373.

[10] Whitfield, T. R.; Wang, X.; Liu, L.; Jacobson, A. J. *Solid State Sci.* **2005**, *7*, 1096.

[11] Mowat, J. P. S.; Miller, S. R.; Slawin, A. M. Z.; Seymour, V. R.; Ashbrook, S. E.; Wright, P. A. *Microporous Mesoporous Mater.* **2011**, *142*, 322.

[12] Millange, F.; Guillou, N.; Walton, R. I.; Greneche, J.-M.; Margiolaki, I.; Ferey, G. *Chem. Commun.* **2008**, 4732.

[13] Devic, T.; Salles, F.; Bourrelly, S.; Moulin, B.; Maurin, G.; Horcajada, P.; Serre, C.; Vimont, A.; Lavalley, J.-C.; Leclerc, H.; Clet, G.; Daturi, M.; Llewellyn, P. L.; Filinchuk, Y.; Ferey, G. *J. Mater. Chem.* **2012**, *22*, 10266.

[14] Mowat, J. P. S.; Seymour, V. R.; Griffin, J. M.; Thompson, S. P.; Slawin, A. M. Z.; Fairen-Jimenez, D.; Duren, T.; Ashbrook, S. E.; Wright, P. A. *Dalton Trans.* **2012**, *41*, 3937.

[15] Millange, F.; Serre, C.; Guillou, N.; Férey, G.; Walton, R. I. *Angew. Chem. Int. Ed.* **2008**, *47*, 4100.

[16] Llewellyn, P. L.; Horcajada, P.; Maurin, G.; Devic, T.; Rosenbach, N.; Bourrelly, S.; Serre, C.; Vincent, D.; Loera-Serna, S.; Filinchuk, Y.; Férey, G. *J. Am. Chem. Soc.* **2009**, *131*, 13002.

[17] Hamon, L.; Llewellyn, P. L.; Devic, T.; Ghoufi, A.; Clet, G.; Guillerm, V.; Pirngruber, G. D.; Maurin, G.; Serre, C.; Driver, G.; Beek, W. v.; Jolimaître, E.; Vimont, A.; Daturi, M.; Férey, G. r. *J. Am. Chem. Soc.* **2009**, *131*, 17490.

[18] Yang, Q.; Wiersum, A. D.; Jobic, H.; Guillerm, V.; Serre, C.; Llewellyn, P. L.; Maurin, G. *J. Phys. Chem. C* **2011**, *115*, 13768.

[19] Salles, F.; Maurin, G.; Serre, C.; Llewellyn, P. L.; Knöfel, C.; Choi, H. J.; Filinchuk, Y.; Oliviero, L.; Vimont, A.; Long, J. R.; Férey, G. *J. Am. Chem. Soc.* **2010**, *132*, 13782.

[20] Hoffmann, H. C.; Assfour, B.; Epperlein, F.; Klein, N.; Paasch, S.; Senkovska, I.; Kaskel, S.; Seifert, G.; Brunner, E. *J. Am. Chem. Soc.* **2011**, *133*, 8681.

[21] Rabone, J.; Yue, Y.-F.; Chong, S. Y.; Stylianou, K. C.; Bacsa, J.; Bradshaw, D.; Darling, G. R.; Berry, N. G.; Khimyak, Y. Z.; Ganin, A. Y.; Wiper, P.; Claridge, J. B.; Rosseinsky, M. J. *Science* **2010**, *329*, 1053.

[22] Ferey, G. *Z. Anorg. Allg. Chem.* **2012**, *638*, 1897.

[23] Ghoufi, A.; Subercaze, A.; Ma, Q.; Yot, P. G.; Ke, Y.; Puente-Orench, I.; Devic, T.; Guillerm, V.; Zhong, C.; Serre, C.; Férey, G.; Maurin, G. *J. Phys. Chem. C* **2012**, *116*, 13289.

[24] Ghoufi, A.; Maurin, G.; Férey, G. *J. Phys. Chem. Lett.* **2010**, *1*, 2810.

[25] Dubbeldam, D.; Krishna, R.; Snurr, R. Q. *J. Phys. Chem. C* **2009**, *113*, 19317.

[26] Coudert, F. o.-X.; Mellot-Draznieks, C.; Fuchs, A. H.; Boutin, A. *J. Am. Chem. Soc.* **2009**, *131*, 11329.

[27] Triguero, C.; Coudert, F.-X.; Boutin, A.; Fuchs, A. H.; Neimark, A. V. *J. Chem. Phys.* **2012**, *137*, 184702.

[28] Coombes, D. S.; Corà, F.; Mellot-Draznieks, C.; Bell, R. G. *J. Phys. Chem. C* **2008**, *113*, 544.

[29] Triguero, C.; Coudert, F.-X.; Boutin, A.; Fuchs, A. H.; Neimark, A. V. *J. Phys. Chem. Lett.* **2011**, *2*, 2033.

[30] Frenkel, D.; Smit, B. *Understanding Molecular Simulation: from algorithms to applications*; 2nd ed.; Academic Press: San Diego, CA 92101-4495, USA, 2002.

[31] Serre, C.; Bourrelly, S.; Vimont, A.; Ramsahye, N. A.; Maurin, G.; Llewellyn, P. L.; Daturi, M.; Filinchuk, Y.; Leynaud, O.; Barnes, P.; Férey, G. *Adv. Mater.* **2007**, *19*, 2246.

[32] Salles, F.; Ghoufi, A.; Maurin, G.; Bell, R. G.; Mellot-Draznieks, C.; Férey, G. *Angew. Chem. Int. Ed.* **2008**, *47*, 8487.

[33] Bourrelly, S.; Moulin, B.; Rivera, A.; Maurin, G.; Devautour-Vinot, S.; Serre, C.; Devic, T.; Horcajada, P.; Vimont, A.; Clet, G.; Daturi, M.; Lavalley, J.-C.; Loera-Serna, S.; Denoyel, R.; Llewellyn, P. L.; Férey, G. *J. Am. Chem. Soc.* **2010**, *132*, 9488.

[34] Salles, F.; Bourrelly, S.; Jobic, H.; Devic, T.; Guillerm, V.; Llewellyn, P.; Serre, C.; Ferey, G. r.; Maurin, G. *J. Phys. Chem. C* **2011**, *115*, 10764.

[35] Hamon, L.; Leclerc, H.; Ghoufi, A.; Oliviero, L.; Travert, A.; Lavalley, J.-C.; Devic, T.; Serre, C.; Férey, G. r.; De Weireld, G.; Vimont, A.; Maurin, G. *J. Phys. Chem. C* **2011**, *115*, 2047.

[36] Zhang, L.; Hu, Z.; Jiang, J. *J. Am. Chem. Soc.* **2013**, *135*, 3722.

[37] Vanduyfhuys, L.; Verstraelen, T.; Vandichel, M.; Waroquier, M.; Van Speybroeck, V. *J. Chem. Theory Comput.* **2012**, *8*, 3217.

[38] Car, R.; Parrinello, M. *Phys. Rev. Lett.* **1985**, *55*, 2471.

[39] Mark, E. T. *J. Phys.: Condens. Matter* **2002**, *14*, R1297.

[40] Kirchner, B.; Dio, P.; Hutter, J. In *Multiscale Molecular Methods in Applied Chemistry*; Kirchner, B., Vrabec, J., Eds.; Springer: Berlin Heidelberg, 2012; Vol. 307, p 109.

[41] Sieffert, N.; Bühl, M.; Gaigeot, M.-P.; Morrison, C. A. *J. Chem. Theory Comput.* **2012**, *9*, 106.

[42] Kimmel, G. A.; Baer, M.; Petrik, N. G.; VandeVondele, J.; Rousseau, R.; Mundy, C. J. *J. Phys. Chem. Lett.* **2012**, *3*, 778.

[43] Mallik, B. S.; Siepmann, J. I. *J. Phys. Chem. B* **2010**, *114*, 12577.

[44] Schmidt, J.; VandeVondele, J.; Kuo, I. F. W.; Sebastiani, D.; Siepmann, J. I.; Hutter, J.; Mundy, C. J. *J. Phys. Chem. B* **2009**, *113*, 11959.

[45] Poater, A.; Ragone, F.; Correa, A.; Cavallo, L. *J. Am. Chem. Soc.* **2009**, *131*, 9000.

[46] Kanoo, P.; Reddy, S. K.; Kumari, G.; Haldar, R.; Narayana, C.; Balasubramanian, S.; Maji, T. K. *Chem. Commun.* **2012**, *48*, 8487.

[47] Schroder, C. A.; Baburin, I. A.; van Wullen, L.; Wiebcke, M.; Leoni, S. *CrystEngComm* **2013**, *15*, 4036.

[48] Cohen, A. J.; Mori-Sánchez, P.; Yang, W. *Chem. Rev.* **2011**, *112*, 289.

[49] Wright, P. A.; Mowat, J. P. S. University of St. Andrews, *Personal communication*, 2013.

[50] Kristyán, S.; Pulay, P. *Chem. Phys. Lett.* **1994**, *229*, 175.

[51] Klimes, J.; Michaelides, A. *J. Chem. Phys.* **2012**, *137*, 120901.

[52] Stavitski, E.; Pidko, E. A.; Couck, S.; Remy, T.; Hensen, E. J. M.; Weckhuysen, B. M.; Denayer, J.; Gascon, J.; Kapteijn, F. *Langmuir* **2011**, *27*, 3970.

[53] Surble, S.; Serre, C.; Mellot-Draznieks, C.; Millange, F.; Ferey, G. *Chem. Commun.* **2006**, 284.

[54] Devic, T.; Horcajada, P.; Serre, C.; Salles, F.; Maurin, G.; Moulin, B.; Heurtaux, D.; Clet, G.; Vimont, A.; Grenèche, J.-M.; Ouay, B. L.; Moreau, F.; Magnier, E.; Filinchuk, Y.; Marrot, J.; Lavalley, J.-C.; Daturi, M.; Férey, G. *J. Am. Chem. Soc.* **2009**, *132*, 1127.

[55] Stylianou, K. C.; Rabone, J.; Chong, S. Y.; Heck, R.; Armstrong, J.; Wiper, P. V.; Jelfs, K. E.; Zlatogorsky, S.; Bacsa, J.; McLennan, A. G.; Ireland, C. P.; Khimyak, Y. Z.; Thomas, K. M.; Bradshaw, D.; Rosseinsky, M. J. *J. Am. Chem. Soc.* **2012**, *134*, 20466.

[56] Levine, B. G.; Stone, J. E.; Kohlmeyer, A. *J. Comput. Phys.* **2011**, *230*, 3556.

[57] Vimont, A.; Travert, A.; Bazin, P.; Lavalley, J.-C.; Daturi, M.; Serre, C.; Ferey, G.; Bourrelly, S.; Llewellyn, P. L. *Chem. Commun.* **2007**, 3291.

[58] Strutt, N. L.; Fairen-Jimenez, D.; Iehl, J.; Lalonde, M. B.; Snurr, R. Q.; Farha, O. K.; Hupp, J. T.; Stoddart, J. F. *J. Am. Chem. Soc.* **2012**, *134*, 17436.

[59] Fairen-Jimenez, D.; Colon, Y. J.; Farha, O. K.; Bae, Y.-S.; Hupp, J. T.; Snurr, R. Q. *Chem. Commun.* **2012**, *48*, 10496.

[60] Bury, W.; Fairen-Jimenez, D.; Lalonde, M. B.; Snurr, R. Q.; Farha, O. K.; Hupp, J. T. *Chem. Mater.* **2013**, *25*, 739.

[61] Bourrelly, S.; Llewellyn, P. L.; Serre, C.; Millange, F.; Loiseau, T.; Férey, G. *J. Am. Chem. Soc.* **2005**, *127*, 13519.

[62] Llewellyn, P. L.; Bourrelly, S.; Vagner, C.; Heymans, N.; Leclerc, H.; Ghoufi, A.; Bazin, P.; Vimont, A.; Daturi, M.; Devic, T.; Serre, C.; Weireld, G. D.; Maurin, G. *J. Phys. Chem. C* **2012**, *117*, 962.

[63] VandeVondele, J.; Krack, M.; Mohamed, F.; Parrinello, M.; Chassaing, T.; Hutter, J. *Comput. Phys. Commun.* **2005**, *167*, 103.

[64] Lippert, B. G.; Parrinello, J. H.; Michele *Mol. Phys.* **1997**, *92*, 477.

[65] Goedecker, S.; Teter, M.; Hutter, J. *Phys. Rev. B* **1996**, *54*, 1703.

[66] Hartwigsen, C.; Goedecker, S.; Hutter, J. *Phys. Rev. B* **1998**, *58*, 3641.

[67] Krack, M. *Theor. Chem. Acc.* **2005**, *114*, 145.

[68] VandeVondele, J.; Hutter, J. *J. Chem. Phys.* **2007**, *127*, 114105.

[69] Becke, A. D. *Phys. Rev. A* **1988**, *38*, 3098.

[70] Lee, C.; Yang, W.; Parr, R. G. *Phys. Rev. B* **1988**, *37*, 785.

Grimme, S.; Antony, J.; Ehrlich, S.; Krieg, H. *J. Chem. Phys.* **2010**, *132*, 154104.